FRACTURE BEHAVIOR OF LARGE-SCALE THIN-SHEET ALUMINUM ALLOY*

Roland deWit, Richard J. Fields, Leonard Mordfin,
Samuel R. Low, and Donald Harne
Mechanical Properties and Performance
National Institute of Standards and Technology
Gaithersburg, MD 20899

ABSTRACT

A series of fracture tests on large-scale, pre-cracked, aluminum alloy panels is being carried out to examine and to characterize the process by which cracks propagate and link up in this material. Extended grips and test fixtures were specially designed to enable the panel specimens to be loaded in tension, in a 1780-kN-capacity universal testing machine. Twelve panel specimens, each consisting of a single sheet of bare 2024-T3 aluminum alloy, 3988 mm high, 2286 mm wide, and 1.016 mm thick are being fabricated with simulated through-cracks oriented horizontally at mid-height. Using existing information, a test matrix has been set up that explores regions of failure that are controlled by fracture mechanics, with additional tests near the boundary between plastic collapse and fracture. In addition, a variety of multiple site damage (MSD) configurations have been included to distinguish between various proposed linkage mechanisms. All tests but one use anti-buckling guides. At this writing seven specimens have been tested. Three were fabricated with a single central crack, three others had multiple cracks on each side of the central crack, and one had a single crack but no anti-buckling guides. Each fracture event was recorded on film, video, computer, magnetic tape, and occasionally optical microscopy. The visual showed the crack tip with a load meter in the field of view, using motion picture film for one tip and SVHS video tape for the other. The computer recorded the output of the testing machine load cell, the stroke, and twelve strain gages at 1.5 second intervals. A wideband FM magnetic tape recorder was used to record data from the same sources. The data were analyzed by two different procedures, (1) the plastic zone model based on the residual strength diagram, and (2) the R-curve. The first three tests were used to determine the basic material properties, and these results were then used in the

---

*Work done under Interagency Agreement No. DTFA03-92-Z-00018, Task Number 4, with the Federal Aviation Administration, U.S.Department of Transportation.

analysis of the two subsequent tests with MSD cracks. There is good agreement between measured values and results obtained from the model.

KEY WORDS: aluminum, crack, fracture mechanics, multiple site damage, plastic zone, R-curve, toughness

INTRODUCTION

The aging of the commercial transport fleets around the world is of constant concern because of the loss of structural integrity through fatigue cracking. In one design approach for aircraft fuselages using semi-monocoque construction, circumferential rings or frames are intended to steer dangerous longitudinal cracks—if they appear—in the less threatening circumferential direction around the fuselage. It has been hypothesized, however, that in the case of aging aircraft in which multiple site damage, such as short fatigue cracks emanating from rivet holes, is present, cracks that start running longitudinally may continue to do so because the cracked rivet holes may provide a path of lesser resistance. Our research is intended to provide some of the information needed to better understand this crack propagation process. In this work we were greatly aided by the advice of David Broek. Also a team from NASA Langley under leadership of James C. Newman assisted with additional measurements.

The specialized facilities and capabilities at NIST are being used to carry out a series of fracture tests on twelve large-scale, 2286-mm wide, pre-cracked, aluminum alloy panels to examine and to characterize the process by which cracks propagate and link up in this material. The tests are sponsored by the Federal Aviation Administration (FAA) as part of its National Aging Aircraft Research Program. The current tests were deemed necessary by the FAA because in previous work [1] only 508-mm wide flat panels were tested, while all other tests were performed on 2286-mm wide curved panels loaded by pressure, both with and without frames and tear straps. The results of these previous tests were predicted very well with a plastic zone model, but showed that the main mode of failure was plastic collapse. In the current program the wide plates failed under conditions closer to fracture mechanics and R-curve behavior.

Using existing information obtained from the tests with smaller specimens, we set up a test matrix that explores regions of failure that are controlled by fracture mechanics, with additional tests near the boundary between plastic collapse and fracture. In addition, a variety of multiple site damage (MSD)

configurations have been included to distinguish between various proposed linkage mechanisms. All tests but one are planned with the use of anti-buckling guides. The one without anti-buckling guides was recommended by NASA Langley to help assess the effect of buckling.

At this writing seven specimens have been tested. Three were fabricated with a single central crack. Three others had multiple cracks on each side of the central crack. One had a single crack with no anti-buckling guides. Each fracture event was recorded on film, video, computer, magnetic tape, and the NASA team occasionally also added optical microscopy. Using flat sheets without stringers to stiffen the panels, these are uncomplicated tests aimed more at obtaining basic material properties than simulating fracture in an airplane fuselage. The material properties sought are the basic fracture properties and linkage criteria for the MSD cracks.

The data were analyzed by two different procedures, (1) the plastic zone model based on the residual strength diagram, and (2) the R-curve. The plastic zone model is an engineering approach which takes the plasticity into account by using an effective fracture toughness, which is less than the true fracture toughness of the material. The basic concept is that the residual strength in the presence of MSD depends on the criterion that an MSD crack will be absorbed by the main crack when their two plastic zones meet, so that the ligament then fails by collapse. It has been a very good predictor of the test results. The R-curve uses a more fundamental approach but requires more data collection and analysis.[1] It accounts directly for the plasticity by the R-curve behavior, and gives more detailed information of the fracture event, such as the amount of crack growth before instability.

The first three tests each contained a single crack and the collected data were used to determine the basic material properties, namely the collapse strength and the effective fracture toughness for the residual strength diagram, and an analytic expression for the R-curve. These results were then used in the analysis of the two subsequent tests with MSD cracks. The results show good agreement between measured values and results obtained from the two independent analyses.

DESCRIPTION OF TESTS

Since this effort uses 90 inch (2286 mm) wide panels, some with multiple site damage (MSD), it has been named the "90 MSD" program. The planned test matrix is shown in Table 1. The

quantities that appear in this table are defined in Figure 2. The individual tests are labeled MSD-1, MSD-2, etc.

Twelve panels were procured, each consisting of a single sheet of bare (not clad) 2024-T3 aluminum alloy, 3988 mm high, 2286 mm wide, and 1.016 mm thick. The specimens are being fabricated with simulated through-cracks oriented horizontally at mid-height. The simulated cracks are saw cuts, ending with the sharpest jeweller's saw cuts available, having a final tip radius of 0.076 mm. The first three tests each had a single central crack. Subsequent tests will also have multiple small cracks on each side of a larger central crack to simulate multiple site damage (MSD). Each MSD crack had a circular 5.6 mm diameter hole in its center to simulate a rivet hole, as shown schematically in Figure 1.

A review of the literature suggests that the specimens tested in this program are the largest structural panels that have been tested in tension. The great size necessitated special design and testing considerations in order to introduce the test loads uniformly along the panel widths. A whiffle-tree approach was ruled out by the height limitations of the 1780-kN-capacity 4-screw-powered universal testing machine (UTM) that was used. As it was, 76 mm had to be cut from the specimens reducing their height to 3912 mm, and only 30 to 50 mm of the testing machine's stroke remained at specimen failure. The machine is one of the largest electro-mechanical testing machines in the world. In its unaltered state, with power screws in all four corners of the 1068 mm x 1524 mm testing table, loads to 448 kN can be applied up to 914 mm off-center, and up to full capacity at 152 mm off-center.

However, to accommodate our large panels, the heads of the testing machine were effectively enlarged with pairs of wide flange structural steel beams (W8x40), 2286 mm long, bolted together. The grips consisted of 2286-mm-long, thick-walled aluminum-alloy extrusions bolted to the steel beams. Each end of the panel specimens was fastened between the grips with forty-five 15.875-mm high-strength steel bolts, fully tightened. The length of the panel between the top and bottom rows of bolts was 3810 mm. Abrasive cloth was inserted between the specimens and the grips to maximize the transfer of load by shear and thereby avoid pin bearing failures of the thin panel material.

The uniformity with which the load was introduced was monitored in the first test with 20 strain gages and in subsequent tests with 10 strain gages mounted on each panel about 406 mm from the grips at each end. These are called the far field strain gages. The strain distribution was measured at low loads, prior to each test, and, if necessary, thin metal shims were inserted between the steel beams and the grips in order to achieve a more uniform distribution. Uniformities within ±10 percent were obtained in

all cases.

Anti-buckling guides, consisting of four aluminum channels, were used to restrain out-of-plane buckling of the panel. The beams were placed horizontally about 12 mm above and below the crack on both sides of the specimen. In the first test a 12 mm thick felt pad was used between the guides and the specimen to facilitate smooth sliding. In subsequent tests rubber was used. Test MSD-6 was performed without the anti-buckling guides to ascertain their effect.

The tests were highly instrumented. Eight additional strain gages (12 for the first test) were placed near the crack tips or MSD cracks. The strain gage signals were run through wide band strain gage conditioning amplifiers. A displacement gage was installed at the bottom of the cross head to measure the total displacement. For specimens MSD-4 and MSD-5 a clipgage was also mounted at the middle of the central crack. The signals of all these gages were recorded by a computer. A SVHS video camera was mounted to view the right crack tip and a motion picture camera viewed the left. For tests MSD-2, 3, 4 and 6 a team from NASA Langley also used high resolution optical microscopy at the left crack tip from the backside. Test MSD-6, which had no anti-buckling guides, used thirteen 3-element rosette strain gages. Seven of these were in the two crack paths and four were near the center of the crack.

The tests consisted of pulling the specimen to fracture under displacement control. The displacement was generally applied at load intervals of 20 to 45 kN and held for one to four minutes at each load level. The whole test lasted from 15 to 20 minutes. Link-ups to MSD cracks occurred in a fraction of a second. Towards the end of the test there was a large amount of crack growth with very small increase of load. After 50 to 100 mm of such tearing instability occurred and the load started to drop. Final fracture occurred with an audible rip.

DATA COLLECTION

The data collection had some built-in redundancy and consisted of up to five components: manual, visual, computer, magnetic tape, and occasionally optical microscopy. The signals from various gages were recorded as a voltage and therefore prior to each test various calibrations were performed to be able to convert these voltage readings to the appropriate physical quantities.

Manual Recording

During the test at each load level the load was noted from the dial of the universal testing machine (UTM). The strain at these loads was read with a bridge amplifier at some of the far field gages near the top and bottom of the specimen. For tests MSD-1 and 7 all the far field strain gages were manually recorded and for MSD-6 none were manually recorded. These recordings provided a record of the average strain and its uniformity across the panel. When the final fracture occurred the fracture load was also recorded from the dial of the UTM.

Visual Recording

The visual recording consisted of showing a voltmeter with a crack tip and the MSD cracks (when present) in the field of view, using SVHS video tape for right tip and motion picture film for the other. The two voltmeters were connected to the UTM load cell and showed a voltage proportional to the load. A calibration was run for the voltmeters prior to the test. The SVHS recording could be observed live on a TV screen. Thus the progress of the crack growth could be monitored during the test. After the test the visual recordings were used to determine the crack extension as a function of the load.

Computer Recording

A personal computer was set up to collect data from various sources. These included the current time, the load obtained from the UTM load cell, the displacement, the strains from the far field gages that were not taken manually, the gages near the crack, and for tests MSD-4, 5, and 7 the clipgage. Each data set was taken at 1½ second intervals, was shown live on the monitor screen, and could be stored in a file.

As mentioned the input data were read as a voltage. Therefore, calibrations were run prior to each test. For the load calibration a simulated load was generated at the UTM console with 22.2 kN intervals from zero up to 200 or 450 kN. The displacement gage was calibrated at 0.254 and 0.635 mm intervals over a range of 20 mm. The strain gages had a resistance of 350 Ω and a gage factor of 2.135. They were calibrated using the

strain gage conditioning amplifiers, which also contained bridge resistances of 350 Ω. With a switch a shunt resistance of 174.8 kΩ could be shorted across the bridge, which corresponded to a simulated strain change of 936 microstrain. The above calibrations resulted in linear conversions. The clipgage worked on the capacitive principle and was calibrated at 0.635 mm intervals from zero to 15 mm. It resulted in a nonlinear conversion of the form $a+bx+cx^2/x+d/x$.

Tape Recording

A wideband FM magnetic tape recorder was used to record data from the same sources as the computer recording. The tape recorder was set to IRIG I and run at 30 inch per second, which provides a distortion free signal (1 dB) from DC to 20 kHz. These recordings are fast enough to show dynamic effects. These data have not yet been analyzed.

Optical Microscopy

For tests MSD-2, 3, and 4 a team from NASA Langley collaborated with high resolution optical microscopy (OM) at one crack tip. For test MSD-6 they additionally recorded the signals from the 3-element rosette strain gages. Their optical microscopy apparatus was used to observe the growing crack. A photographic technique was developed to measure the crack tip opening angle during crack initiation and stable tearing. The OM apparatus consisted of a computer controlled, long focal length microscope fitted to a video camera. The field of view of the microscope was a square with sides approximately 1.8 mm long. The field of view was centered on the crack tip and advanced as the crack grew. The results from this analysis will be reported elsewhere by NASA Langley.

R-CURVE ANALYSIS

The crack extension that occurred as the load increased was measured with the SVHS video tape, the movie film, and the OM apparatus. The results for tests MSD-1, 2, 3 and 6 are shown in Figure 3. These tests all had a single central crack, see Table

C-6

1. Specimen MSD-6 had no anti-buckling guides and the data for this test fall below those for MSD-3, which had the same crack size. This shows that the lack of guides and consequent buckling acted as a stress intensification at the crack tips.

We have used the R-curve concept [2] to analyze some of the data. First, we show here how to find the crack-extension force, G, from the slow stable crack growth data. This quantity is related to the stress-intensity factor, K, by

$$G = K^2/E \tag{1}$$

where E is Young's modulus. The stress-intensity factor is generally given by the generic expression

$$K = \beta\sigma\sqrt{(\pi a)} \tag{2}$$

where the function β is used to describe the effect of the shape and size of the crack and the specimen. For the center crack specimen we then have

$$G(a) = (\sigma^2\pi a/E)\beta^2(\pi a/W) \tag{3}$$

where σ is the applied stress, a the half-crack size, and W the panel width. For the stress-intensity factor of a center-notch specimen with sharp crack tips Feddersen [3] discovered that

$$\beta(\pi a/W) = \sqrt{\sec(\pi a/W)} \tag{4}$$

gives an approximation that is accurate to 0.3 percent for $2a/W<0.7$. The stress is given by

$$\sigma = P/(WB) \tag{5}$$

where P is the load and B is the panel thickness. For our panels we have

$$W = 2286 \text{ mm}$$
$$B = 1.016 \text{ mm}$$
$$E = 71 \text{ GPa}$$

Using these values and Equations (3)-(5), the movie film and video tape data from Figure 3 were converted into the crack-extension force data shown in Figure 4. We see that for small crack-extensions the data from the tests with the anti-buckling guides collapse nicely into a master curve, but without anti-buckling guides the data are distinctly different. Now, according to the R-curve concept the crack-extension resistance, R, equals the crack-extension force, G, for slow stable crack growth with a sharp crack tip. We wish to identify those points for tests MSD-1, 2, and 3, shown solid in Figure 4, that qualify as R-curve data. The data with no crack-extension represent the

original blunt notch and so do not yet represent crack growth along the R-curve. For short crack-extensions up to about 75 mm there is slow stable crack growth, while for larger crack-extensions there is unstable dynamic crack growth. Initially we do not yet know the critical point of instability that separates the stable from the unstable data for each test. We therefore used an iterative procedure and started with an initial guess for the critical crack-extension. To represent the R data by a universal R-curve, a power law was fitted to them, giving

$$R = 75.9\ da^{0.28} \tag{6}$$

where R is measured in kN/m and da in mm. With an analytic expression for the R-curve the point of instability can be found. The stability diagram in Figure 5 illustrates this for test MSD-1. A crack-extension force line or G-line is drawn and the control parameter is adjusted until the line is tangent to the R-curve when it becomes the G_c-line. For simplicity we can take for G the expression for the infinite plate with a single crack (β=1) under load or stress control

$$G = \sigma^2 \pi a/E \tag{7}$$

because for cracks under 500 mm in our panels this equation does not differ much from the correct expression below. Equation (7) gives a straight line in Figure 5. Tangency is achieved by adjusting the stress until a critical value of σ_c=146 MPa is obtained, which then gives a critical crack-extension of da_c=69.3 mm and a critical crack-extension force of G_c=249 kN/m. Hence, the data points for which 0<da<69.3 mm are stable for MSD-1 and those points were used for the curve fit in Figure 4. The same procedure was applied to the data of tests MSD-2 and 3. If it is found that the initial guess for da_c was wrong the procedure is repeated until all the fitted points lie below the points of tangency. Figure 5 shows that for da>da_c the unstable points lie closer to the G_c-line than the R-curve.

Actually the testing machine was operated under displacement control so that the displacement, δ, is the control parameter. This quantity is related to the stress by

$$\sigma = \delta/(BWC_t) \tag{8}$$

where C_t is the total compliance of the testing system, which can be decomposed into the machine, panel, and crack compliance, as follows

$$C_t = C_m + H/(EBW) + 4/(\pi EB)\ I(\pi a/W) \tag{9}$$

where H (150 in) is the panel height and

$$I(x) = \int x\beta(x)dx \tag{10}$$

The total compliance was found for each test from the slope of the measured total displacement versus load curve. Using the slope before any crack extension occurred, Equation (9) was used to deduce the machine compliance. The average for the first three tests was $C_m = 1.082 \times 10^{-5}$ m/kN (± 4%). The complete expression for the G-line under displacement control is then given by combining Equations (3), (8), and (9) into

$$G(a) = E\delta^2 \pi a \, \beta^2(\pi a/W) \; / \; [EBWC_m + H + 4W/\pi \; I(\pi a/W)]^2 \qquad (11)$$

To find the critical point of instability, as was done in Figure 5, the displacement is adjusted in this equation until tangency to the R-curve is achieved. In this way critical values are found for the displacement, δ_c, crack-extension, da_c, and crack-extension force, G_c. The critical stress, σ_c, is found by Equation (8) or (3), the load, P_c, by Equation (5), and the toughness, K_c, by Equation (1). The results for the first three tests are summarized in Table 2. This table also includes measured values and results from the residual strength diagram discussed in the next section. There is good agreement.

RESIDUAL STRENGTH DIAGRAM

The residual strength diagram is used in an engineering approach to determine how the residual strength of a structure depends on the crack geometry and the specimen size. It is shown schematically for a center cracked sheet structure in Figure 6. The dotted line represents the residual strength assuming linear elastic fracture mechanics for an infinite sheet. The straight line shows the residual strength assuming net section collapse of a sheet of width W. For small and large crack sizes, near the intersections of these two curves there is a region of transition from one failure mode to the other. Feddersen [4] argued that two linear tangents to the idealized K curve can be used to establish a smooth and continuous curve for the residual strength. One tangent to the K curve is drawn from the point $\sigma=\sigma_Y$, where σ_Y is the stress at which the structure without crack collapses. The other tangent is drawn from the point 2a=W that represents the width of the structure. The fracture toughness is customarily determined from the crack size at the failure stress by Equation (2). However, in thin sheets where crack extension occurs before failure, the final crack size is generally not known. Therefore the data points plotted in the residual strength diagram usually are the initial crack size and the final failure stress, i.e. the crack extension and plasticity are ignored. To compensate for this inconsistency, an effective value of the toughness is used, denoted by K_e, which is lower than the true toughness, such as that obtained e.g. by the R-

curve. A slight improvement to the analysis can also be made by taking the finite width of the panel into account, i.e. by using

$$K_e = \sigma_c[\pi a_i \sec(\pi a_i/W)]^{1/2} \quad (12)$$

In this way a value of K_e=111 MPa$\sqrt{m}$ was obtained as the average of the first three tests. Application of the residual strength diagram to the first three tests is shown in Figure 7. The predicted fracture paths are shown and the measured data points are plotted as solid circles. The results for all three tests fall in the fracture mechanics region of the diagram. They are summarized in Table 2. There is good agreement between the measured data, the predictions from the R-curve and the residual strength diagram for these single crack specimens.

THE LINK-UP CRITERION

For the panels with multiple site damage (MSD) we have used the analysis of Broek [1]. Here we have a situation where small cracks exist ahead of the large central crack. The first link-up is governed by the stress-intensity factor of the combination of the main crack and the first MSD crack. The geometry factors of the two cracks must therefore be compounded by the effect of crack interaction. As the ligament undoubtedly will fail by plastic collapse or net section yield, the compounded stress intensity factor can be used to calculate the plastic zone of both cracks and used with the criterion that link-up occurs when the two plastic zones meet. Broek found that the best estimate of the plastic zone size for this application was given by the Irwin expression

$$r_p = (K/\sigma_Y)^2/2\pi \quad (13)$$

where σ_Y is the collapse strength. This expression represents the plastic zone at the tip of the main crack and a similar expression holds for the plastic zone at the MSD crack. Here the stress-intensity factor is still given by Equation (2), but with the MSD crack nearby the function β that takes the crack interaction into account is much more complicated than Equation (4). To model the first link-up Broek assumed that the main interaction was between one tip of the central crack and the first MSD crack in front of it, ignoring all the other MSD cracks. Thus β will depend on the central crack size, a, the MSD crack size, a_{MSD}, and the ligament L between them, Figure 2, so that Equation (2) becomes

$$K = \beta(a, a_{MSD}, L)\ \sigma\sqrt{(\pi a)} \quad (14)$$

A similar expression holds for the stress-intensity factor to use in the plastic zone at the MSD crack. For these β functions Broek has derived approximations based on published expressions for the stress intensity factors of two unequal length collinear cracks, which we have used. The link-up criterion between the central and first MSD crack now is

$$r_p + r_{pMSD} = L \tag{15}$$

or, from Equations (13) and (14)

$$\sigma = \sigma_Y[2L/(a\beta^2 + a_{MSD}\beta_{MSD}^2)]^{1/2} \tag{16}$$

For test MSD-4 this expression is plotted as the first dashed curve in Figure 8. Though it is not shown explicitly in Equation (16) this curve represents the final failure stress as a function of initial crack size, in the same sense as was discussed for Equation (12). The x-axis in Figure 8 represents the central crack size, a. For the curves that are plotted the MSD crack size, a_{MSD}, and the position of the MSD crack, d_{MSD}, are kept constant. However, as may be clear from Figure 2, the ligament L varies with a. For the central crack with size a=177.8 mm, Equation (16) predicts the first link-up at σ=81 MPa. This is shown by the intersection of the fracture path line with the first dashed curve in Figure 8. After the first link-up the central crack has absorbed the first MSD crack and it is assumed that we now have a larger central crack, a=195.58 mm, that interacts with the second MSD crack. Equation (16) is again used with these new parameters and plotted as the second dashed curve in Figure 8. The predicted stress for the second link-up then is σ=117 MPa. This procedure is then repeated for the third link-up and we find σ=111 MPa at a=220.98 mm. Since this stress is lower than for the second link-up, we conclude that the panel is super-critical and the fracture will run straight through after absorbing the second MSD crack at 117 MPa, as shown by the fracture path in Figure 8. When all three MSD cracks have been absorbed by the central crack, it behaves as a large single crack of size a=246.38 mm in the panel. Failure is then predicted by the simpler Equation (12), as also shown in Figure 8. The results of this analysis for tests MSD-4, 5, and 7 are summarized in Table 3 and compared with the measured values.

R-CURVE AND MSD

We now apply the R-curve to the failure prediction of a panel with MSD cracks. We assume that an R-curve emanates from each MSD crack as well as the main central crack, as shown by the solid lines in Figure 9. Each R-curve is given by Equation (6).

We then draw G_c-lines tangent to each R-curve to determine the link-ups and final instability. The G-lines are still given by an expression similar to Equation (3), but now the β function for the central crack must also take the interaction with the MSD crack into account

$$G(a) = (\sigma^2 \pi a/E)\beta^2(a, a_{MSD}, L) \quad (17)$$

For a given stress this equation gives the G-line under load control. Using the appropriate parameters, the stress was adjusted until tangency was achieved for each of the R-curves, as shown by the dashed lines in Figure 9. The final fracture at 246.3 mm uses the same procedure as discussed before. With the MSD cracks the G-lines have quite a bit of curvature just before the instability point. The link-up stress for the third MSD crack is less than for the second. This indicates that, after link-up of the second MSD crack, the panel is super-critical and the fracture will run straight through after absorbing the second MSD crack. The results for tests MSD-4, 5, and 7 are summarized in Table 3. There is good agreement with the measured values and also with the results predicted from the plastic zone model. However, for MSD-5 and 7 the prediction from both the R-curve and the plastic zone model is that the final fracture will occur with the second and third link-up, whereas actually the load had to be raised from 375 to 407 kN for MSD-5 and from 205 to 214 kN for MSD-7 after the second and third link-ups for the final fracture.

CONCLUSION

Analysis appears to provide good predictions of the residual strength, link-ups, and fracture of panels with multiple site damage (MSD) of different size and spacing. The critical fracture stress can be predicted by using either the plastic zone criterion or the R-curve, and the results are virtually the same. Several improvements to the analysis are being considered. Notwithstanding the large widths of the panels the MSD cracks are quite small and closely spaced so that small discrepancies in these dimensions may affect the results. Therefore more accurate measurements of the MSD configurations are currently being made under a microscope. The plastic zone analysis uses guestimates for the effective fracture toughness, K_e, and the collapse strength, σ_y. The values of these two quantities can be optimized when the data from all the tests are in. In the R-curve analysis load control was used and the backward growth of the MSD crack was ignored. Improvements in this analysis are quite complex, but we think possible. Displacement control would allow the load to drop as in fact it did in MSD-5 and 7.

REFERENCES

1. Broek, D., "The effects of multi-site damage on the arrest capability of aircraft fuselage structures," FractuREsearch TR 9302, June 1993

2. Broek, D.: Elementary Engineering Fracture Mechanics. Martinus Nijhoff Publishers, 1987

3. Feddersen, C. E.: "Discussion," Plane Strain Crack Toughness Testing of High Strength Metallic Materials, ASTM STP 410, by William F. Brown, Jr., and John E. Srawley, American Society for Testing and Materials, Philadelphia, 1966, p. 77

4. Feddersen, C. E.: "Evaluation and prediction of the residual strength of center cracked tension panels," ASTM STP 486, American Society for Testing and Materials, Philadelphia, 1971, pp. 50-78

Table 1. Planned Test Matrix for 90 MSD Program

Test No	Main crack		MSD cracks				Date of test
	2a (mm)	a (mm)	d_{MSD} (mm)	s_{MSD} (mm)	$2a_{MSD}$ (mm)	number per side	
MSD-1	355.6	177.8				0	7/23/93
MSD-2	203.2	101.6				0	8/25/93
MSD-3	508.0	254.0				0	9/13/93
MSD-4	355.6	177.8	190.5	25.4	10.16	3	11/29/93
MSD-5	142.24	71.12	88.9	38.1	15.24	3	12/1/93
MSD-6[A]	508.0	254.0	(no anti-buckling guides)				4/12/94
MSD-7	508.0	254.0	266.7	38.1	12.7	5	4/20/94
MSD-8[B]	355.6	177.8	190.5	25.4	10.16	3	
MSD-9	482.6	241.3	266.7	38.1	12.7	10	
MSD-10	254.0	127.0	165.1	25.4	10.16	10	
MSD-11	(to be defined)						
MSD-12	(to be defined)						

[A] This test was recommended by NASA Langley
[B] This test is a repeat of MSD-4

Table 2. Measured Data and Failure Predictions for the First Three 90 MSD Tests

	Half-Crack Size			Stress (MPa)	Load (kN)	Displacement (mm)	
	Initial (mm)	Final (mm)	Extension (mm)				Date
MSD-2							
Measured	101.6			184	428	16.1	8/25/93
RSD		142	40.4	196	454		
R-curve		141.1	39.5	183	424	14.5	
MSD-1							
Measured	177.8			148	343	12.6	7/23/93
RSD		244.3	66.5	146	340		
R-curve		247.1	69.3	146	340	11.9	
MSD-3							
Measured	254.0			124	289	12.2	9/13/93
RSD		340.4	86.4	121	280		
R-curve		353.1	99.1	125	289	10.5	

Table 3. Link-up and Failure Predictions from the Residual Strength Diagram and the R-curve for tests 90 MSD-4, 5, and 7

	Link-up 1		Link-up 2		Link-up 3		Fracture	
	Load (kN)	Stress (MPa)	Load (kN)	Stress (MPa)	Load (kN)	Stress (MPa)	Load (kN)	Stress (MPa)
MSD-4								
Measured	196	84	227	98	227	98	307	132
RSD	188	81	272	117	(258)	(111)	285	123
R-curve	240	103	274	118	(258)	(111)	294	126
MSD-5								
Measured	320	138	375	161	375	161	407	174
RSD	329	142	445	191	(392)	(169)	(346)	(149)
R-curve	388	167	403	174	(347)	(149)	(344)	(148)
MSD-7								
Measured	133	57	205	88	205	88	214	92
RSD	134	57.8	268	116	(249)	(107)	(204)	(88)
R-curve	183	78.9	255	110	(239)	(103)	(213)	(92)

The numbers in parentheses are lower than for a previous link-up, thus failure will precede the link-up

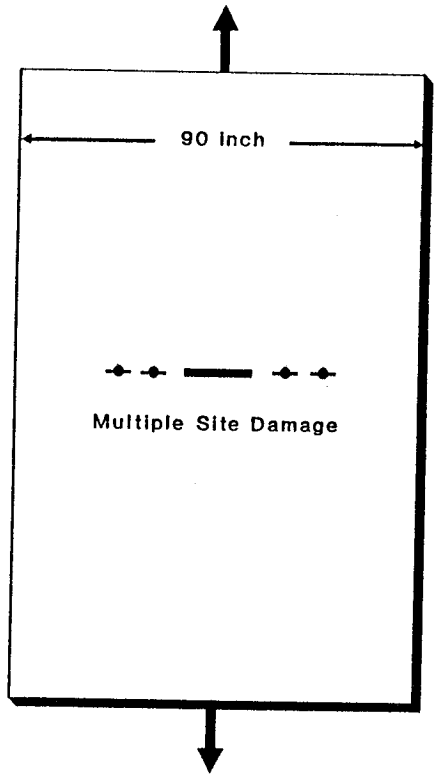

Figure 1. Typical 90 MSD test panel

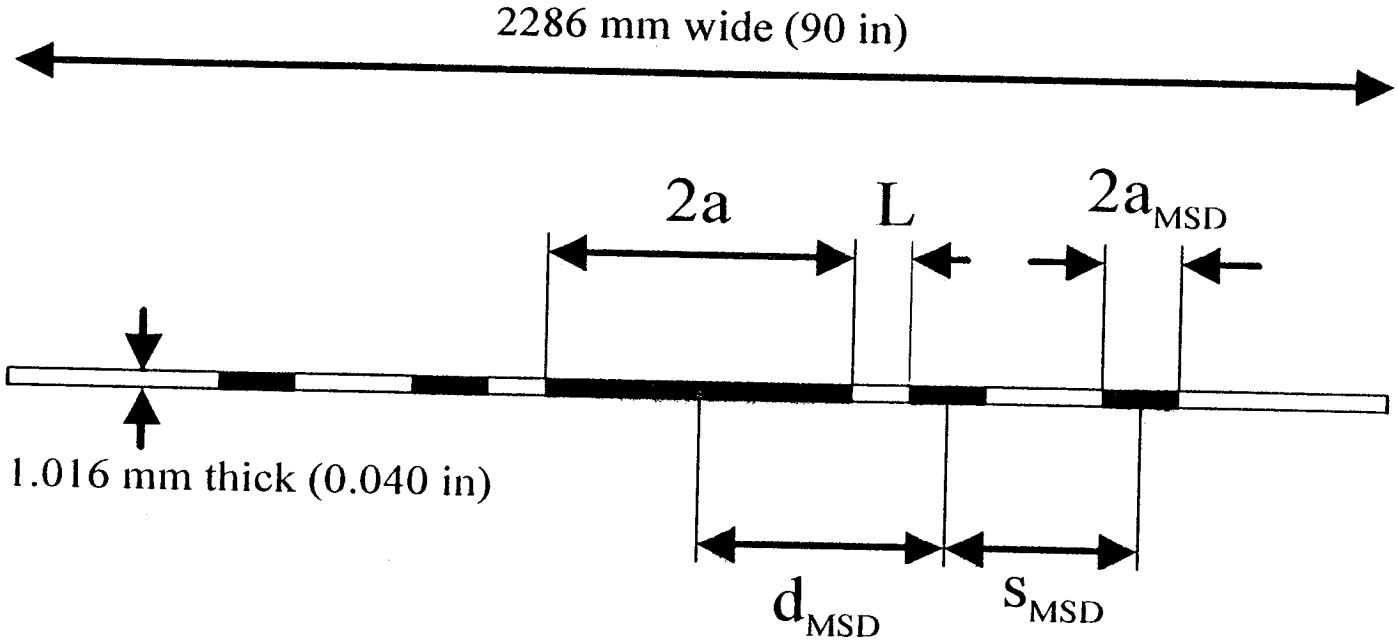

Figure 2. Definitions of 90 MSD crack configurations and dimensions

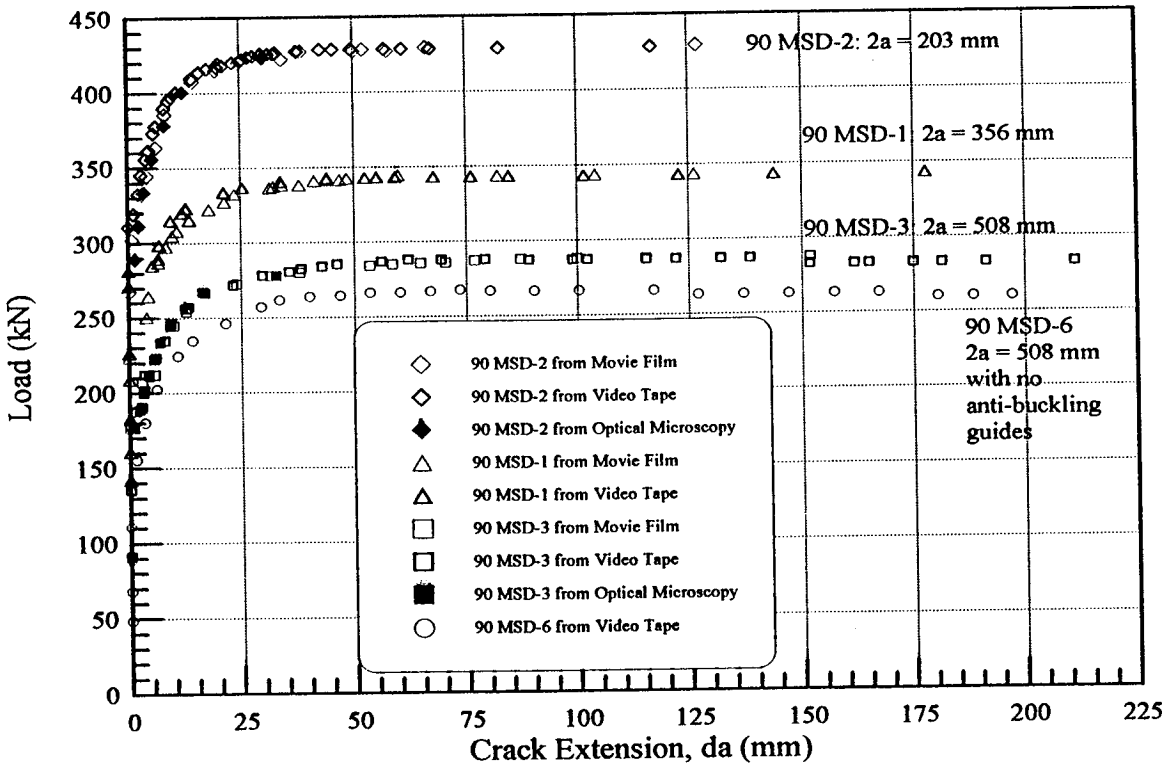

Figure 3. Crack growth measurements for tests 90 MSD-1, 2, 3 and 6

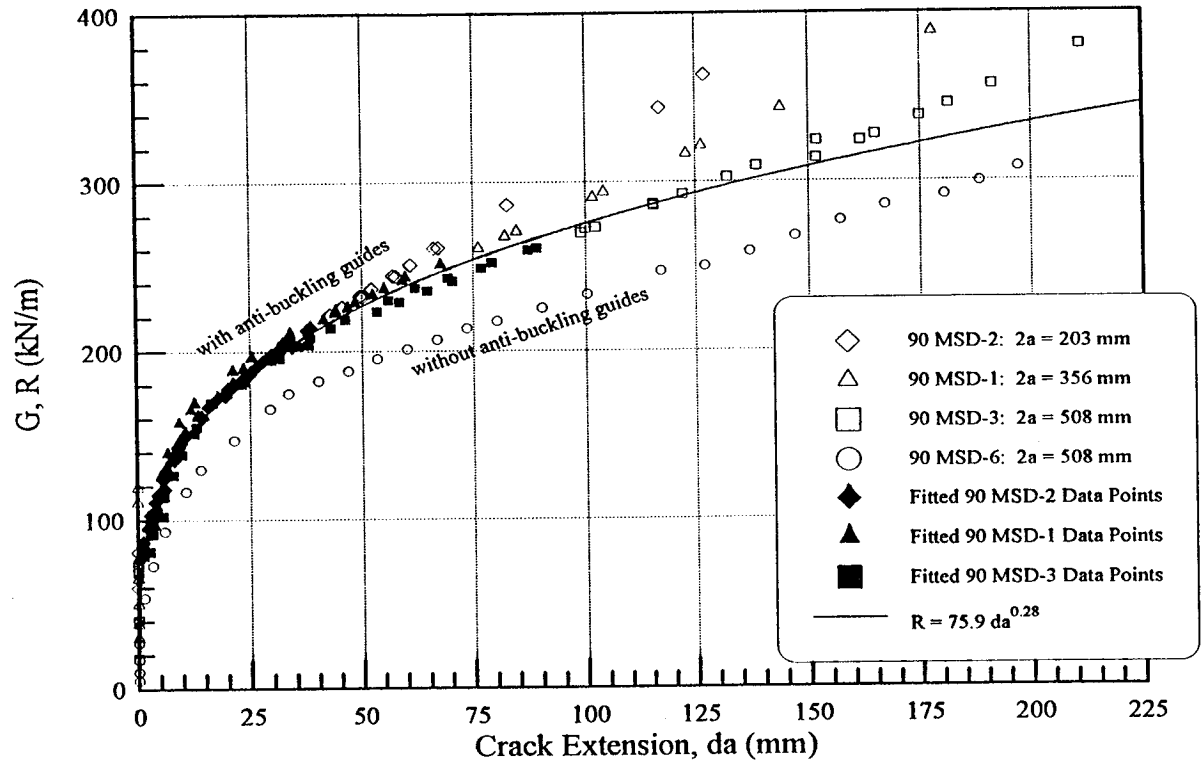

Figure 4. Crack-extension force data and analytic R-curve for 90 MSD tests

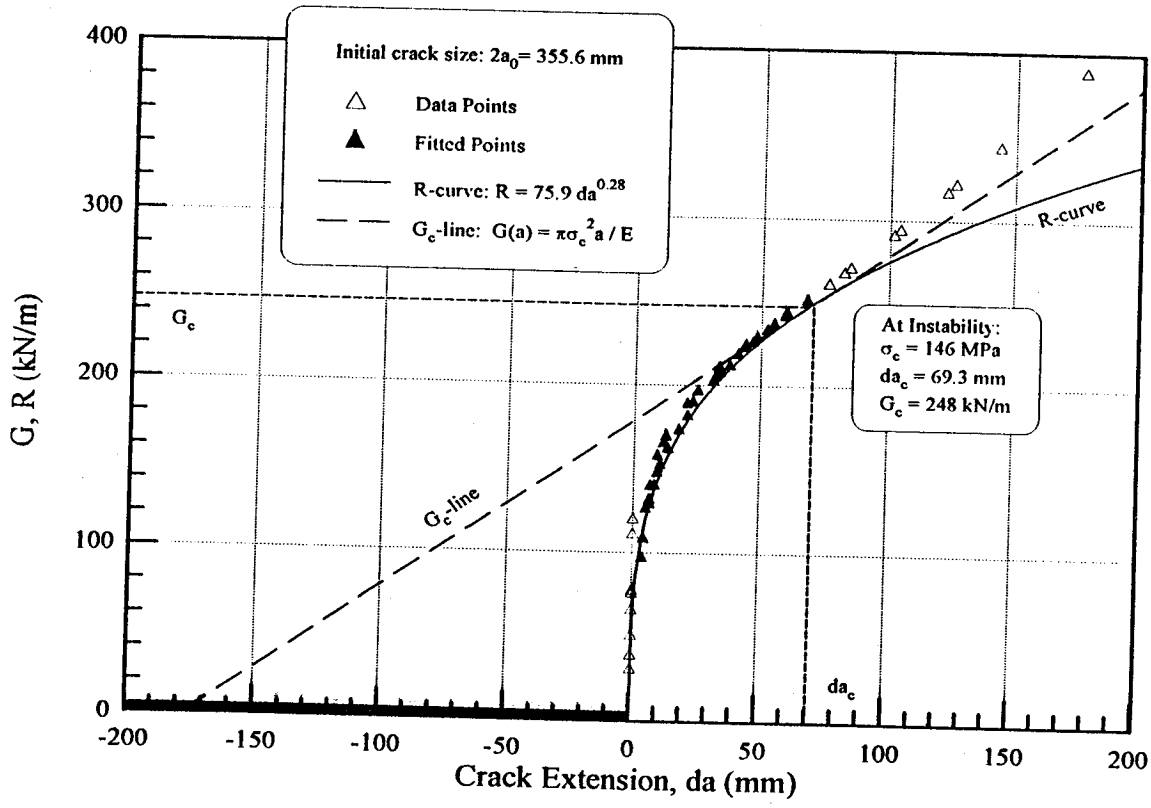

Figure 5. Stability diagram for test 90 MSD-1

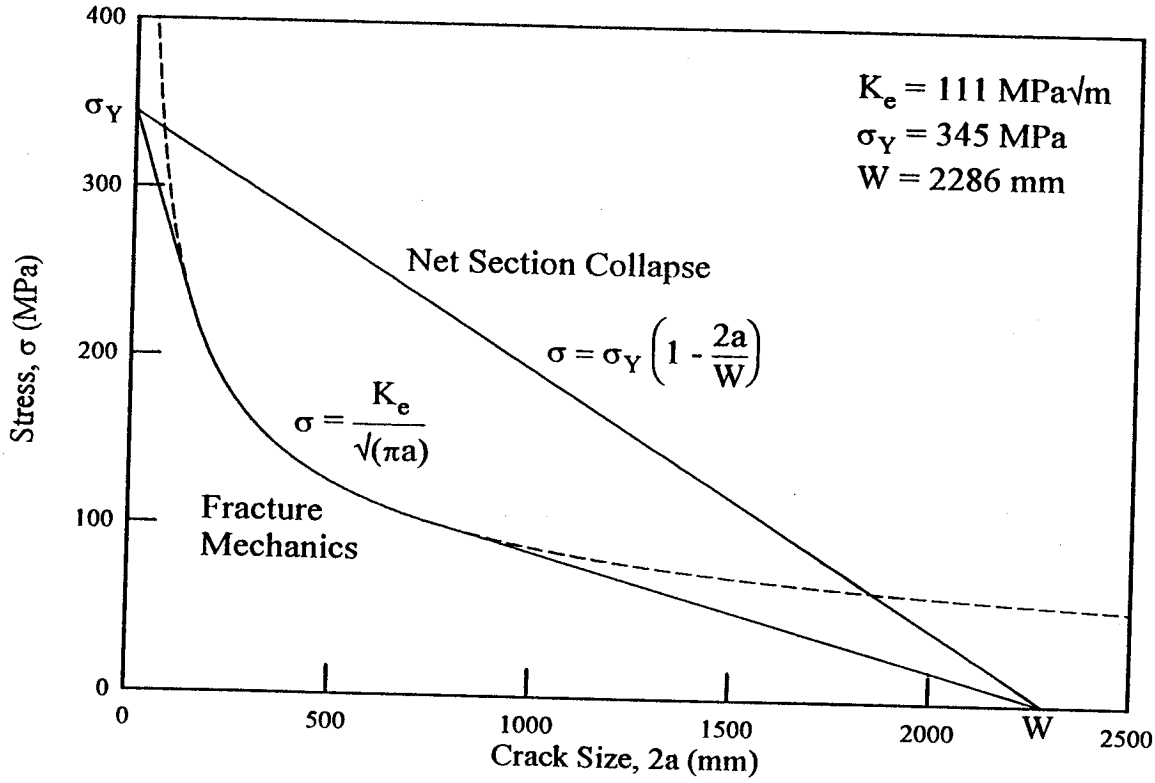

Figure 6. Residual strength diagram with analysis of Feddersen

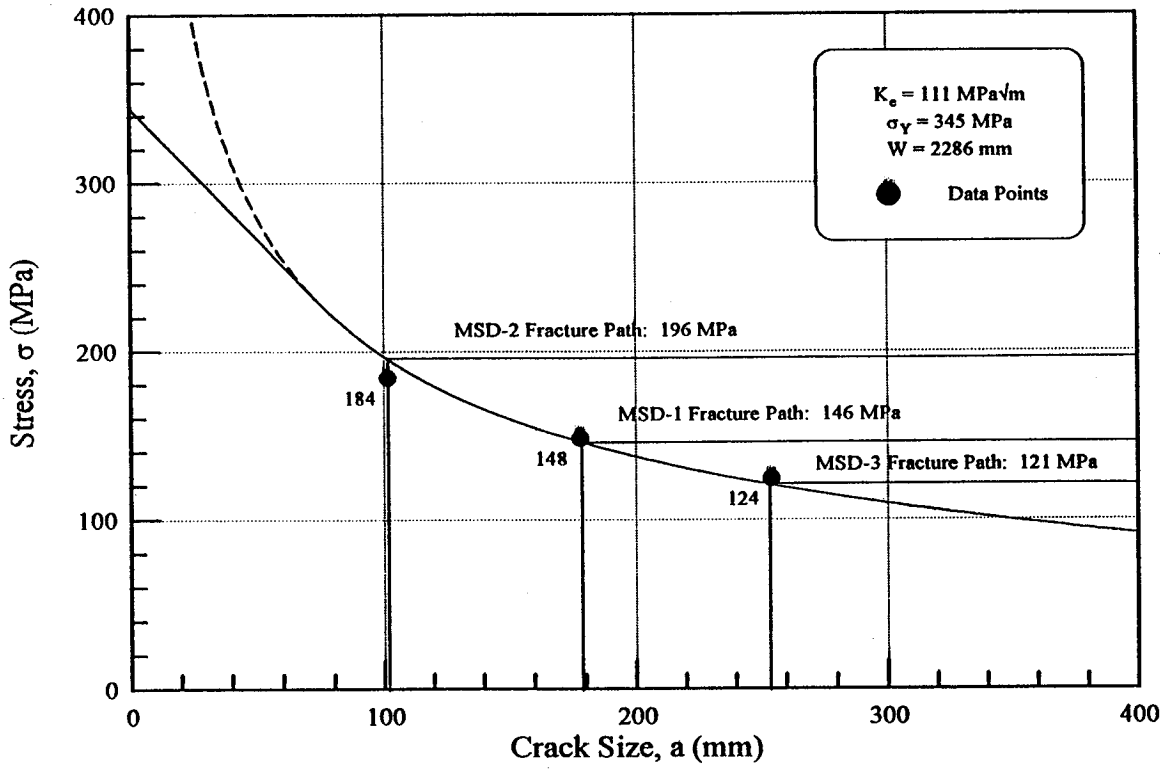

Figure 7. Residual strength for tests MSD-1,2, and 3 with measured data points and predicted fracture paths

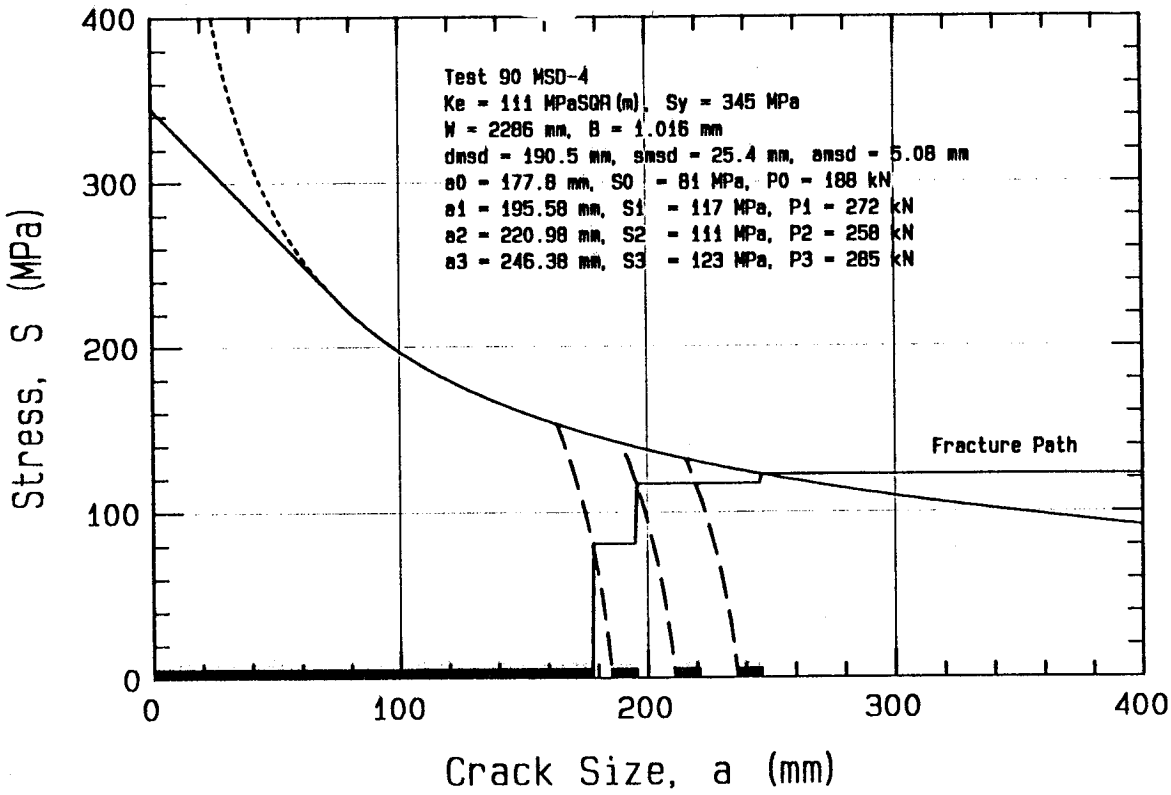

Figure 8. Residual strength diagram for test MSD-4 with plastic zone criteria and predicted fracture path

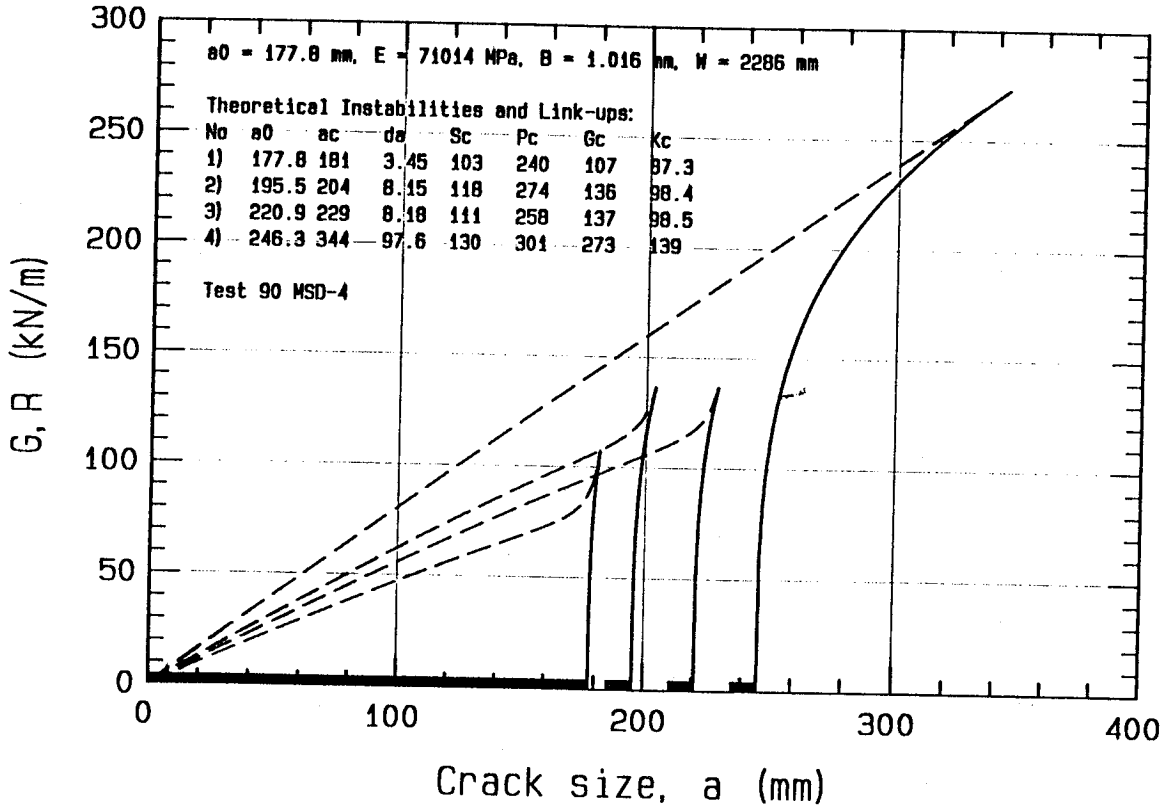

Figure 9. Stability diagram for test 90 MSD-4